Web Intelligence and Agent Systems: An International Journal 12 (2014) 63–82
DOI 10.3233/WIA-140286
IOS Press

Foundations of automatic system for intrasurgical localization of subthalamic nucleus in Parkinson patients

Konrad A. Ciecierski [a,*], Zbigniew W. Raś [a,b] and Andrzej W. Przybyszewski [c]
[a] *Warsaw Univ. of Technology, Institute of Comp. Science, 00-655 Warsaw, Poland*
[b] *Univ. of North Carolina, Dept. of Comp. Science, Charlotte, NC 28223, USA*
[c] *UMass Medical School, Dept. of Neurology, Worcester, MA 01655, USA*

Abstract. During deep brain stimulation (DBS) treatment of Parkinson disease, the target of the surgery is the subthalamic nucleus (STN). This anatomical structure is small ($9 \times 7 \times 4$ mm) and poorly visible using Computer Tomography (CT) or Magnetic Resonance Imaging (MRI) scans.

Because of that, a multi-electrode micro recording system is used intra surgically for better localization of the target nucleus. This paper presents five different analytical methods, that can be used to construct an autonomic system which can aid neurosurgeons in precise localization of the $Subthalamic\ Nucleus$ (STN). Such system could be used during surgery in the environment of the operation theater. Described methods take as input signals recorded from the micro electrodes. Their result in turn allows one to tell which from the recorded signals comes from the STN. First method bases on the recorded action potentials, i.e. on electrical activity of neurons that are near electrode's recording tip. Second utilizes root mean square of recorded signals. Third takes into account amplitude of the background noise present in the recorded signal. The last two methods examine Low Frequency Background (LFB) and High Frequency Background (HFB).

Keywords: Parkinson's disease, DBS, STN, FFT, DWT, RMS, LFB, HFB, hierarchical clustering

1. Introduction

Parkinson disease (PD) is chronic and advancing movement disorder. The risk factor of the disease increases with the age. As the average human life span elongates also the number of people affected with PD steadily increases. Because of the nature of the illness – affecting only patient's movement without impairment of the intelligence and/or consciousness – it has a very high social cost. People as early as in their 40s, having unaffected mental capabilities are seriously disabled and require continuous additional external support. The main treatment for the disease is pharmacological one. Unfortunately, in many cases the effectiveness of the treatment decreases with time and some others patients do not tolerate anti PD drugs well. In such cases, after fulfilling certain medical requirements patients are qualified for the surgical treatment of the PD disease. This kind of surgery is called Deep Brain Stimulation (DBS). Goal of the surgery is the placement of the permanent stimulating electrode into the STN nucleus. This nucleus is a small – deep in brain placed – structure that does not show well in CT or MRI scans. Stimulating electrode disrupts overactive neural circuits that are responsible for the forming of the rigidness typical for the advanced stage of the PD disease. Having only an approximate location of the STN, during DBS surgery a set ($3\sim5$) of parallel micro electrodes are inserted into patient's brain. Electrodes are directed towards expected location of the target nucleus. At each desired depth they record electrophysiological activity of surrounding brain tis-

*Corresponding author. E-mail: K.Ciecierski@ii.pw.edu.pl.

sue. Micro electrodes advance until at least one of them passes through the nucleus, determining by this its $dorsal$[1] and $ventral$[2] borders. All this is possible because STN has distinct from surrounding tissue physiology and yields specific micro electrode recordings. It still requires however an experienced neurologist/neurosurgeon to tell whether recorded signal comes from the STN or not [1].

When the trajectory to the STN and its depth are in this way obtained, electrodes are withdrawn to its level. Then the ones that reached it in an optimal way are one by one briefly switched from recording to stimulation mode. While stimulation is active, patients condition is monitored and effectiveness of treatment assessed. By this procedure optimal electrode is determined and later all micro electrodes can be withdrawn. Subsequently, using the trajectory of the optimal micro electrode, the final and permanent stimulating electrode is placed.

Required experience of the neurologist/neurosurgeon can cause certain difficulties. That is why it is so important to provide some objective and human independent way to discriminate recorded signals. The goal is to provide the human independent software that would be able to assess in a short time whether given recording has originated inside of the STN or not.

Analytical methods described in this paper have been devised with exactly that purpose. Taking as input recordings made by set of electrodes at subsequent depths they provide information as to which of the electrodes and at which depth passed through the STN.

2. Related work

2.1. Signal filtering

In micro electrode recorded signals filtering is necessary for various reasons. Different methods require different kind of raw signal preprocessing and filtering. Most commonly for filtering used are Fast Fourier Transform (FFT) and Discrete Wavelet Transform (DWT) methods. FFT (Discrete Fourier Transform in case of sampled data) can be used for filtering in many application, it has however some more or less serious disadvantages.

[1] Top.
[2] Bottom.

2.1.1. FFT

FFT is based on a sine wave. This implies that it is best suited for stationary signals, i.e. signals that repeat forever without a change in its periodicity. Meanwhile recordings acquired from the brain tissue are not stationary. One might even say that in some brain areas if neuronal activity starts to behave in a synchronous and stationary way then serious neurological condition might be taking place [2].

Because trigonometrical functions are not timed localized, it is only possible to say what frequencies are dominant in a surveyed signal. It is not possible to tell when these frequencies occurred in time. This comes from FFT's assumption of stationarity of the signal.

When FFT is used for filtering, first the transformation goes forward into frequency domain, later coefficients corresponding to desired frequencies are thresholded and finally the inverse transform goes back to the time domain. As all above is done using sine wave, the resulting filtered signal also acquires some sine like properties. It is especially undesired when one is to analyze and compare the shapes of the action potentials.

2.1.2. DWT

Wavelet transforms do not assume stationarity of the signal. It comes from the fact that wavelet base function is also time localized – not stationary. Because of this, the information regarding time in which certain frequencies are present is preserved. This feature caused DWT to become frequently used in medical signal analysis [3–6]. From this, looking at specific wavelet transform one can easily identify corresponding sample ranges in raw unfiltered signal [7]. FFT is based on a sine wave, in the case of DWT there are many functions that can be used as a base wave. In [8] authors suggest Daubechies D4 wavelet. This wavelet, having its shape akin to simplified spike shape is especially useful in analyzing neurobiological data. Because of that, in this paper wavelet transforms have been used for filtering.

Discrete Wavelet Transform (DWT) is done both in forward and reverse way in steps. Each step in forward transform gives coefficients corresponding to different frequency ranges. As each stage of the transform it is required that input signal has even number of samples. From this comes an obvious requirement that raw input signal has to have length which is a certain power of 2. Of course, the longer is the input signal the more steps of the transform can be made and the more detailed results could be obtained. Assume that raw signal has n samples (numbered 0 to $n-1$) and that it has been

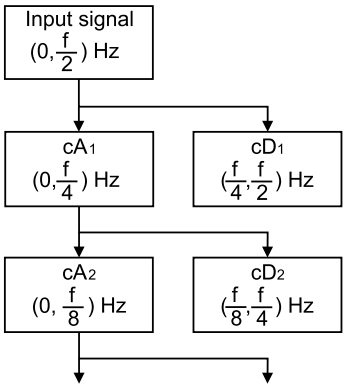

Fig. 1. DWT schema.

sampled with f frequency. From Nyquist theorem [9] the frequency ranges present in the signal are in range $(0, \frac{f}{2})$.

After the 1st step of the transform, coefficients in range $\langle 0, \frac{n}{2} - 1\rangle$ reflect frequencies $(0, \frac{f}{4})$. They are called cA_1 – $average$ of the signal for the 1st level.

Range $\langle \frac{n}{2}, n - 1\rangle$ reflects frequencies $(\frac{f}{4}, \frac{f}{2})$ and it is in analogous way called cD_1 – $detail$ of the signal for the 1st level.

Both cA_1 and cD_1 sets of coefficients contain $\frac{n}{2}$ elements, so each element of cA_1 references two elements of the original signal. This way, while having only half of the elements, they still come from the whole length of the original data. Exactly the same rule takes place in case of the cD_1 coefficients.

Second level takes cA_1 as an input and produces division of $(0, \frac{f}{4})$: range cA_2 is for frequencies $(0, \frac{f}{8})$ and cD_2 is for frequencies $(\frac{f}{8}, \frac{f}{4})$.

Declaring the raw input signal as A_0, one could say that level j is produced as the step forward from A_{j-1}: cA_j represents frequencies $(0, \frac{f}{2^{(j+1)}})$ and cD_j represents frequencies $(\frac{f}{2^{(j+1)}}, \frac{f}{2^j})$.

There is a little point in further transforming data of length 4 or less. Having stated above, one can obtain the maximum possible level of transformation of a signal with n samples, it is $\log_2 n - 2$.

First two steps of the DWT are shown on Fig. 1.

On the Figs 2–6, sample of microelectrode recorded signal is shown together with its first two DWT steps. It is immediately obvious that original signal shape is in some way maintained in cA_1 (Fig. 3) and cA_2 (Fig. 5).

– DWT preserved information about occurrence events in time

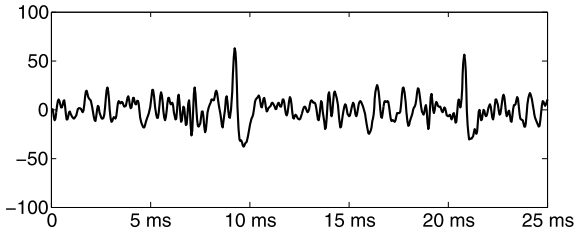

Fig. 2. Raw microelectrode recording (0–12 KHz).

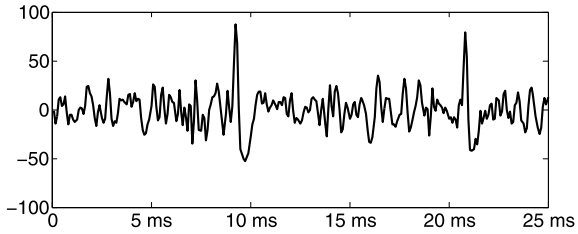

Fig. 3. cA1 (0–6 KHz).

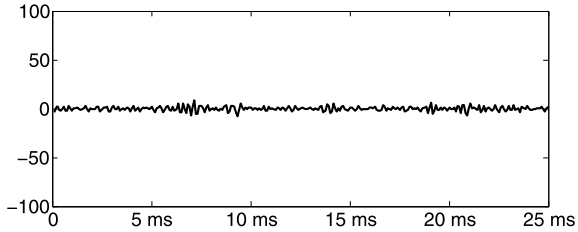

Fig. 4. cD1 (6–12 KHz).

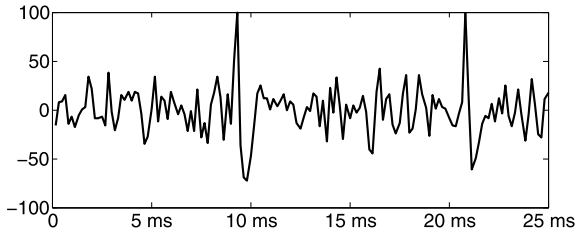

Fig. 5. cA2 (0–3 KHz).

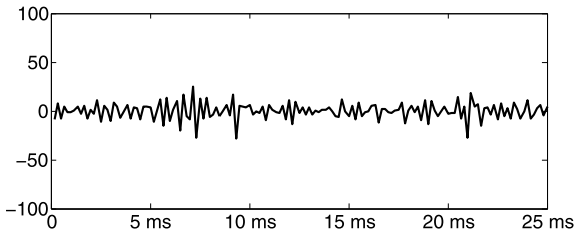

Fig. 6. cD2 (3–6 KHz).

– noise above 6 KHz seems to be insignificant
– noise in range 3∼6 KHz does distort the signal

2.2. Signal's normalization

The need for normalization of the recorded signals comes from several reasons.

1. There is no guarantee that at each depth the length of the recording would be the same. In our data set there are 9685 recordings, 8931 of them (92 %) have length of 10 s, 599 (6 %) are shorter and finally 155 (2 %) are longer than 10 s.

2. Each electrode is used only for one pass through the brain tissue so in each trajectory different electrode is used. While electrodes are in general uniform as to their electrical properties, some small differences can still be present.

3. In different surgeries, different amplification factor can be set in the recording device.

First case – acting on a single recording level – implies that method relying on the power of the signal (Spike based, RMS, LFB and HFB) must be normalized in such way that from a given recording they produce power proportional to 1s of its length. Without that comparing power yielded from i.e. 10 s and 20 s long signals would be meaningless.

Last two reasons – acting on the electrode level – normalizes amplitude of data calculated from full pass of a single electrode. Normalization must allow one to safely compare signals recorded by different electrodes with different amplification factors.

During the DBS surgery electrode starts its recording at level -10000 (10 mm above predicted STN location) and from there follows its tract for another 15 mm to the level $+5000$ (5 mm below predicted STN location). There are also cases when electrode is advanced even beyond level of $+5000$. Important fact is that first 5 mm of the tract produces relatively unform recordings (low amplitude, little or no spiking). Assume now that a specific method mth taking as input vector of data recorded at subsequent depths D produces a vector of characteristic coefficients C.

$$mth(d_{-10000}, \ldots, d_{+5000}) = (c_{-10000}, \ldots, c_{+5000}) \tag{1}$$

The base value of C is then defined as

$$C_{base} = \frac{c_{-10000} + \cdots + c_{-6000}}{5} \tag{2}$$

and, finally the normalized C has form

$$C_{NR} = \left(\frac{c_{-10000}}{C_{base}}, \ldots, \frac{c_{+5000}}{C_{base}} \right) \tag{3}$$

All the results from the methods presented in following sections are normalized according to the length of the recording. All results from the percentile, RMS, LFB and HFB methods are also normalized using Eqs (1)–(3). Spike based method – described in following chapter – does not require electrode level normalization of the resulting coefficients. This is due to the fact, that it does rely on spike occurrence which is not so much dependant on the electrode sensitivity or amplification level. Moreover, in not uncommon situation when at first 5 depths electrode records no spikes, the C_{base} value would be 0 and C_{NR} could not be calculated at all.

2.3. Analysis of the action potentials – spikes

It is possible to detect spikes occurring in cells being within radius of around 50 μm from the electrode's recording tip [10]. Spikes from far neurons may have lower amplitude and be wider. Change of width is caused by the fact that with increasing distance more and more of the spike's high frequency components are lost. Distant neurons contribute to the noise present in the recorded signals. Because of that, spikes coming from two neurons of the same type, with different distance from the electrode can be recorded with both different amplitude and width. Depending on the brain region, within radius of 50 μm one might find well over 100 neurons. This neurons can produce spikes in different patterns and frequencies. It is also not uncommon that couple of neurons produce spikes within few milliseconds of each other and that the recorded spikes would overlap. All above makes the task of detecting and sorting of the spikes particulary difficult.

2.3.1. Objectives

The STN nucleus is a structure within brain that characterizes by large amounts of densely packed neurons [1,2]. It might be so expected that power of the signal that is derived from spike occurrences would reflect that feature. Power of such signal should be therefore higher in the STN than in other brain areas being near it (i.e. Striatum, Dorsal Thalamus, Zona Incerta). Comparing changes of the power for electrodes from given set, on different depths, should provide some information as to which of the electrodes and on what depth traversed the STN.

2.3.2. High pass filtering

Spikes can be detected using amplitude or derivative thresholding. In case of derivative methods one looks for the first derivative being above or below cer-

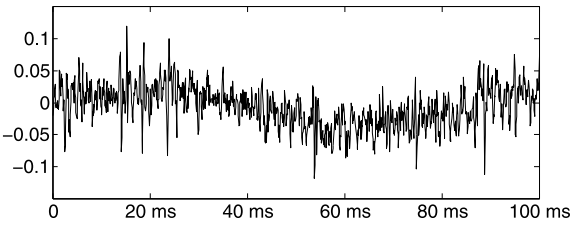

Fig. 7. Recording before DWT hight pass filtering.

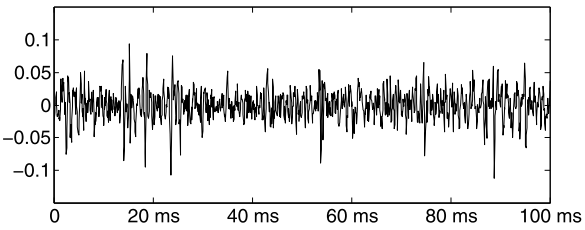

Fig. 8. Recording after DWT hight pass filtering.

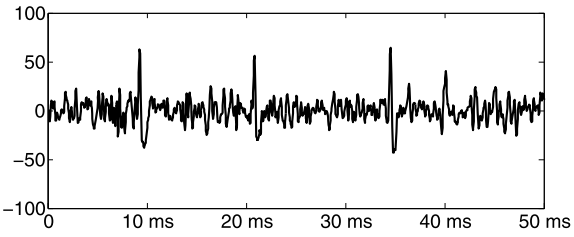

Fig. 9. Recording before DWT low pass filtering.

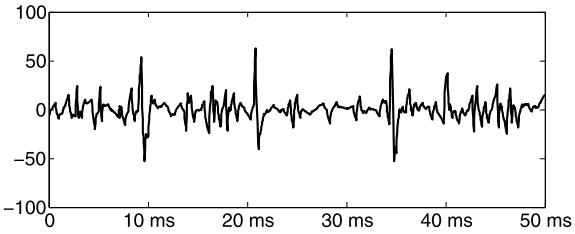

Fig. 10. Recording after DWT low pass filtering.

tain threshold. Spike detection is in this way based on its slope. Unfortunately it is difficult to calculate such thresholds in an automatic unsupervised way. Methods that base on amplitude are easier to implement. For these methods the threshold can be quite easily calculated from the recorded signal. Amplitude approach requires however that the signal has to be firstly high pass filtered.

High pass filtering is done by removing all frequencies below 375 Hz. Having the original signal recorded in ranges $(0, 12)$ KHz we have cA_1 representing frequencies below 6 KHz, cA_2 for frequencies below 3 KHz ... and finally cA_5 that represents frequencies below 375 Hz. Having done all five steps of DWT all cA_5 coefficients are set to 0 and then five consecutive inverse DWT are made. Results of such filtering are shown on Figs 7 and 8. Test sample is a 100 ms long subset of real, MER recorded signal. Signal contains 6 spikes with high amplitude. It is clearly apparent that DWT filtering removed low frequency oscillations without affecting neuronal spikes.

2.3.3. Low pass filtering

In previous sections it has been stated that within the recording radius of the electrode over 100 neurons can be found. Most of these cells are electrically active either by their spikes or by synapse potentials. All this activity contributes to the noise that is always abundant in MER recordings. The more neurons are nearby, the bigger is the noise amplitude. While this feature can itself carry significant information (see Sections 2.5 and 2.6) in case of spike detection and subsequent sorting it is just a distortion and should be removed [11]. In this case, filtering is also done by means of DWT. Noise frequencies are here very close to frequencies present in spikes and because of that they can not be removed by simple zeroing of certain coefficients. Such simple approach, while removing the unwanted noise would also distort spikes.

The signal is instead a decomposed threefold and at each step some hard thresholding is done. At the first level, the detail coefficients cD_1 representing frequencies in range 6 KHz$\sim$12 KHz are hard thresholded with value $4\sigma_n$. At the 2nd level, the detail coefficients cD_2 representing frequencies in range 3 KHz–6 KHz are also hard thresholded with value $4\sigma_n$. Finally, at the 3rd level, the detail component cD_3 representing range 1500 Hz–3 KHz is hard thresholded with value $2\sigma_n$. The value σ_n is given by Eq. (6). Such equation, as pointed in [12] has some advantages over the classical formula that uses average of squares. Mainly, the traditional formula takes into account all samples and is thus strongly affected by high amplitude values that comes form spikes. Formula for hard tresholding x with value λ is given by Eq. (4).

$$htresh(x, \lambda) = \begin{cases} 0 & \text{if } |x| \leq \lambda \\ x & \text{otherwise} \end{cases} \tag{4}$$

Later the transformation process is reversed and filtered signal is thus obtained. Figures 9 and 10 presents a 50 ms wide signal sample before and after the fil-

tering. Low pass filtering considerably improves spike detection and subsequent sorting processes.

2.3.4. Spike detection

Assuming that unwanted frequency components have already been filtered out from the signal, one can attempt to detect spikes using amplitude analysis [13]. Assuming that x_k denotes k_{th} sample of input signal, threshold is V_{thr} set by Eq. (5).

$$V_{thr} = 4\,\sigma \tag{5}$$

where

$$\sigma = \frac{median(|x_1|, \ldots, |x_n|)}{0.6745} \tag{6}$$

Necessary condition for a spike to be detected is that al least one of its samples exceeds V_{thr}. This condition while being a must is certainly not a sufficient one. Neural spike has to fit into certain shape range. To ensure it, additional conditions must be fulfilled, they specify amplitude ranges into which spike amplitude must not enter. As spikes can be recorded both in normal and reverted polarity, two sets of such zones must be defined. This zones of forbidden amplitude are shown on Fig. 11.

In case of *down-up* spikes (see Fig. 11a) the $-V_{thr}$ amplitude is shown as thin horizontal line. Assuming that amplitude is below $-V_{thr}$ at time t_0 then spike occurs between $t_0 - 0.5$ ms and $t_0 + 1.1$ ms if fulfilled are conditions (7)–(10).

$$\forall(t_0 - 0.5_{\mathrm{ms}} < t < t_0 - 0.4_{\mathrm{ms}})\;\; f(t) > -\frac{V_{thr}}{2} \tag{7}$$

$$\forall(t_0 + 0.4_{\mathrm{ms}} < t < t_0 + 1.1_{\mathrm{ms}})\;\; f(t) > -\frac{V_{thr}}{2} \tag{8}$$

$$\forall(t_0 - 0.5_{\mathrm{ms}} < t < t_0 - 0.3_{\mathrm{ms}})\;\; f(t) < \frac{V_{thr}}{2} \tag{9}$$

$$\forall(t_0 + 1.0_{\mathrm{ms}} < t < t_0 + 1.1_{\mathrm{ms}})\;\; f(t) < \frac{V_{thr}}{2} \tag{10}$$

In case of *up-down* spikes (see Fig. 11b) the V_{thr} amplitude is also shown as thin horizontal line. Conditions (7)–(10) have to be here modified in a simple way to reflect reversed polarity.

2.3.5. Shape clustering

After spike detection it is a good practice to separate spikes coming from different neurons. While around 100 of them can be in a vicinity of an electrode only few of them are close enough to yield good

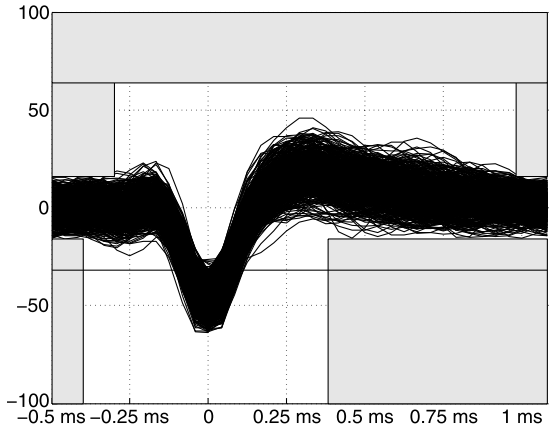

(a) Down-Up spikes

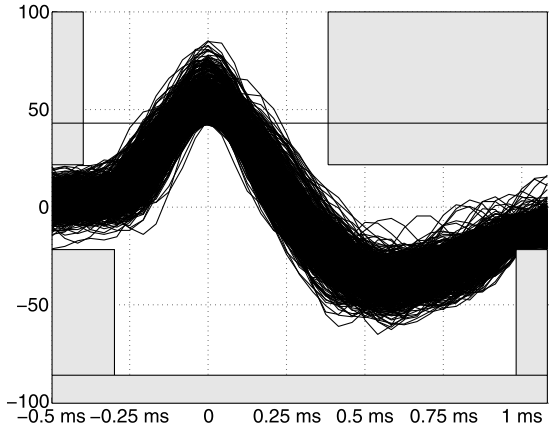

(b) Up-Down spikes

Fig. 11. Forbidden spike amplitude areas, each figure shows over 500 superimposed spikes.

spike recordings. Author in [2] states that shape of a recorded spike depends on:

- physical construction of a cell
- concentration of extracellular Na+ ions
- place in which electrode is relatively close to neuron soma (body)

As none of the above does change during recording process, one can make assumption that spikes of different shapes come from different neurons. [14] Note, that these neurons do not have to be of a different type (see last condition, Section 2.3 and [10]). Clustering of spike shapes it done threefold. In the first step samples containing spikes are transformed using level four Daubechies D1 (Haar) DWT [15]. Second step selects coefficients best suited for final clustering. Selection is done using modified Kolomogorov-Smirnov

test (see [16]). Finally clusters are obtained using $k\text{-}means$ method.

Figure 12 shows example of spike discrimination. In processed recording 554 spikes were found (Fig. 12a). Spikes were subsequently divided into two shape classes containing 440 (Fig. 12b) and 114 (Fig. 12c) spikes.

Distinguished shape classes can be later used ([1], Chapter 12) for obtaining further neuron specific statistics that might be useful in STN localization.

2.3.6. Meta signal construction

Creation of the special temporary meta signal is required because the goal of this method is to obtain power yielded by spikes only. All background noise must be removed. Firstly the meta signal is created with sampling 1 KHz, length equal to this of original recording and with uniform zero amplitude. Later for each spike, having time of its occurrence one can obtain corresponding sample number in the meta signal. Amplitude for such samples is then set to 1 (Dirac's delta), finally signal is convoluted with positive part of cosine. For this cosine function values are mapped in such a way that part of cosine defined on $\langle -\frac{\pi}{2},\ \frac{\pi}{2} \rangle$ is mapped onto 11 samples spanning together 10 ms. These tree steps are shown on Figs 13–15.

2.3.7. Meta signal's power

When all spikes have their representation in the temporary meta signal, it is transformed using FFT to obtain the general power spectrum. As meta signal is sampled 1 KHz, it is possible to obtain power spectrum for frequencies up to 500 Hz. Power of the frequencies above 100 Hz is very small and as frequency increases, it quickly approaches zero. Because of that, only for frequencies less or equal 100 Hz power spectrum is being observed. Power is so calculated for frequency range from 1 Hz to 100 Hz. Assuming that for a given electrode e the power of a meta signal obtained from depth d is calculated for a frequency f, it is represented by $pwr(e,\ d,\ f)$.

Summary power for electrode e at depth d is defined by Eq. (11).

$$pwr_{sum}(e,\ d) = \sum_{f=1}^{100} pwr(e, d, f) \tag{11}$$

During DBS surgery set of electrodes traverse selected hemisphere on parallel trajectories towards the STN. Electrodes record potentials at the same time and for the same time period. It is safe to compare the power of the signal recorded in these electrodes. Having definition for summary power, definition of cumulative power can be introduced. This cumulative power

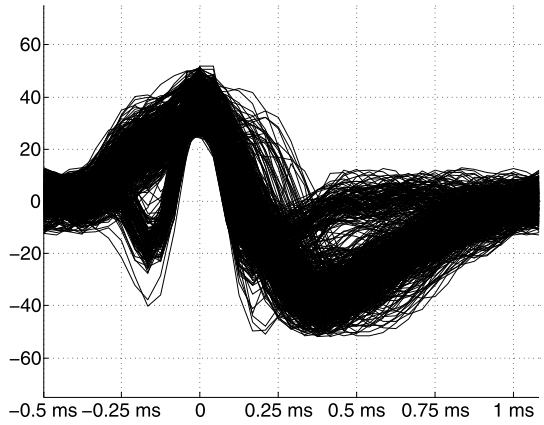

(a) All spikes

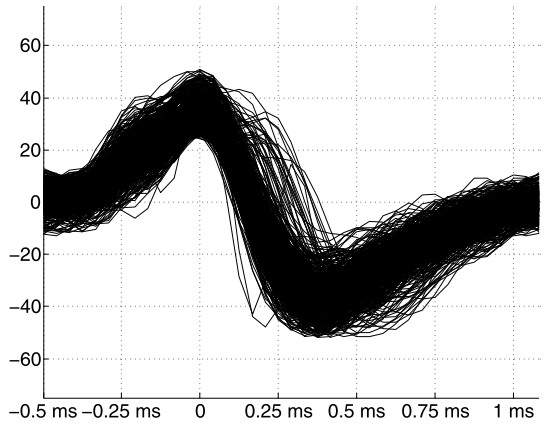

(b) Class A spikes

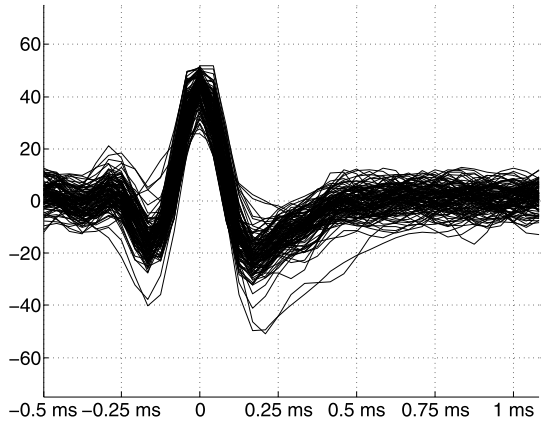

(c) Class B spikes

Fig. 12. An example of the spike discrimination: a) 554 spikes, b) 440 spikes, c) 114 spikes.

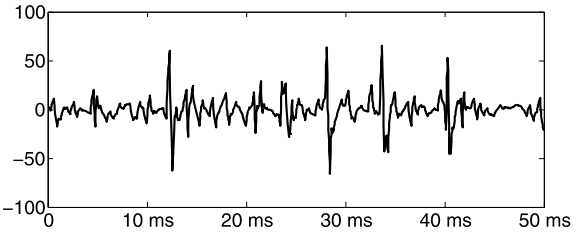

Fig. 13. Filtered microelectrode recording (sample rate 24 KHz).

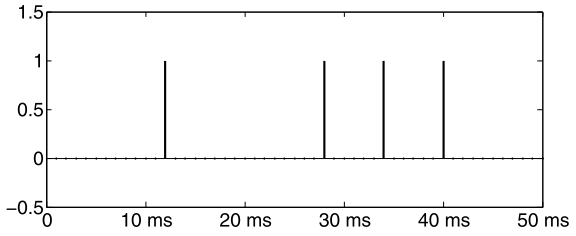

Fig. 14. Meta signal (sample rate 1 KHz).

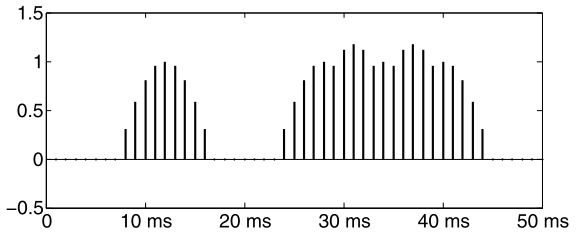

Fig. 15. Convoluted meta signal (sample rate 1 KHz).

is defined by Eq. (12).

$$pwr_{cumul}(e,\ d) = \sum_{d_i \leq d} pwr_{sum}(e,\ d_i) \qquad (12)$$

2.3.8. Results

For each electrode two types of charts can be produced. In both cases X axis shows depths on which recordings has been made, Y axis shows either value of Eq. (11) or (12). Most useful, allowing for quick compare, are charts showing summary or cumulative power together for all electrodes from a given set.

Two such charts are presented on Fig. 16. What is obvious is that power of the spike based signal indeed does reflect increased spiking activity in the STN. Both $posterior$[3] and $central$ electrodes show on Fig. 16a high increase in the summary power, clear indication that both of them reached and traversed the

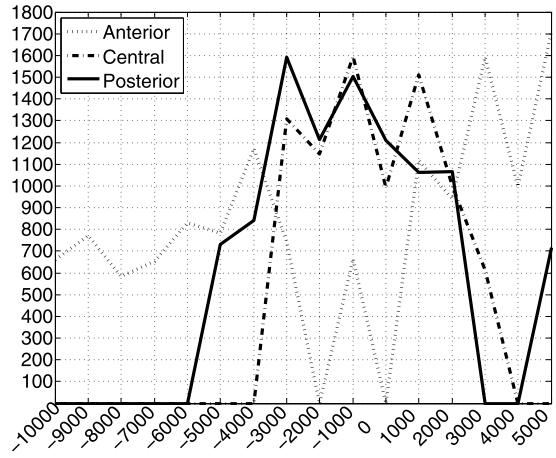

(a) summary power

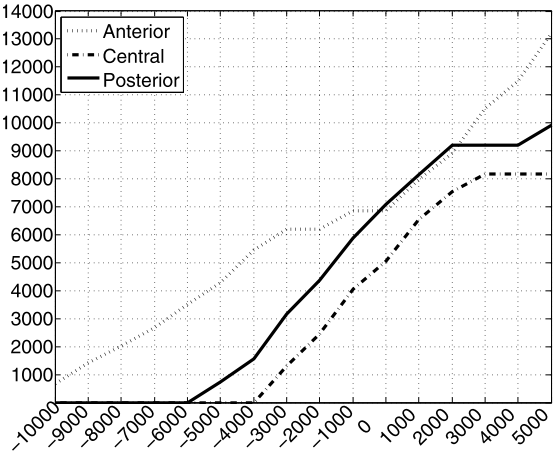

(b) cumulative power

Fig. 16. Power of the meta signal: a) summary power, b) cumulative power.

STN at depth ranging roughly from -3000 (-3 mm) to 1000 ($+1$ mm). Depth zero is the depth of the STN estimated on CT/MRI scans.

The $anterior$[4] electrode shows here somewhat different picture. While starting with elevated power, it shows decrease of it around the depth -3000. Together with finding from two other electrodes one might assume that this electrode probably did miss the target. Big increase of power from $anterior$ electrode that can be observed around the $+3000$ depth can be with high certainty explained by its entering the region called $Substantia\ Nigra$. Zone that lies dorsal to the STN Nucleus is also characterized by spikes

[3] Most backward, closest to the back of the head.

[4] Most forward, closest to the front of the head.

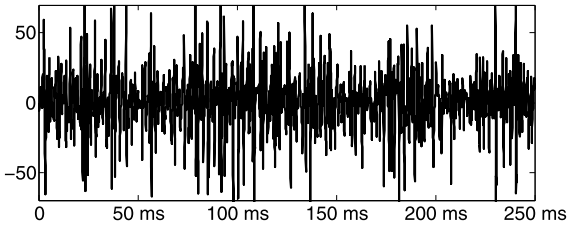

Fig. 17. STN recording.

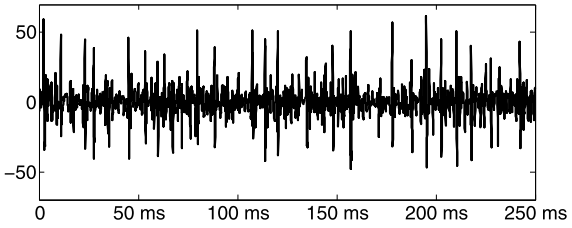

Fig. 18. SNr recording.

with high frequency [1]. While from the results of this method, these two regions i.e. STN and SNr may look similar, they have other feature that differentiate them clearly, as shown on Figs 17 and 18. Other methods described later in following sections take this into account.

Method basing on calculation of meta signal can be used for estimation of the STN's localization. Spike detection criteria ensures that this approach does not suffer from recoded signal contamination by external (i.e. electronic, mechanic) noise. If spike becomes too distorted, it simply would not be qualified. Such noise can only lower the resulting power. So, while it is possible that highly contaminated signal from the STN may have lower power, the other situation – false STN detection – is not probable.

Results base on spikes and by this on their detection process. This introduces also some disadvantages. Mainly there is no guarantee that even in active brain ares, such as STN, electrode will be placed near active cell. It has higher probability in STN, where there are many highly active cells, but still there is no guarantee. That's mainly why the summary power can jump between certain levels on subsequent depths. Such value jumping can be observed on Fig. 16a at depths between -3000 and -1000. This can be in some way amended by using also cumulative power and ordering electrodes by value of that power on deepest level. Electrodes with higher cumulative power more likely have passed through the STN that others.

In specific situations, this measure can be misleading. If specific electrode does not reach the STN but maintains some medium summary power throughout all depth, its cumulative power can still be the greatest one. This drawback does not occur in methods presented in following sections.

Ordering electrodes in such way has also some clinical applications. In some cases, electrode that has been marked as best, either using summary power or cumulative power simply can not be used. This can be due to the presence of adverse clinical observations when such electrode is briefly switched from recording to stimulation. In such case 2nd best electrode is chosen.

2.4. Artifacts removal

Methods described in later sections do not rely on spike detection. They base on data extracted from signal's amplitude or its power for certain frequency ranges. Both amplitude and power analysis are highly affected by signal contamination. Because contaminating noise causes increase in both power and amplitude, its removal is especially important to avoid false STN detections. Most simple solution, used by authors in [17], just ignores all contaminated data. Here, solution to salvage uncontaminated portions of such data has been devised.

Artifacts reside mainly in low frequencies ($<$375 Hz). Normally proper for such frequencies DWT coefficients have uniform and low amplitude. Looking for coefficients with amplitudes exceeding some threshold should therefore provide information about localization of artifacts in a given recording. Time bound relation between DWT coefficients and signal samples allows for artifacts removal.

2.4.1. Removal procedure

If signal reaches maximal allowed amplitude for at least 0.01 % of its samples it is qualified, contaminated, and filtered in a special DWT based way. Six forward steps of DWT are made. Knowing that signal has been sampled with 24 KHz, each coefficient at kth level of DWT corresponds to 2^k samples in the original signal.

- set of cA_6 coefficients corresponding to original's signal in frequency range 0–187 Hz
- set of cD_6 coefficients corresponding to original's signal in frequency range 187–375 Hz

According to Eq. (6) σ_{cA} and σ_{cD} values are calculated from respectively cA_6 and cD_6 sets. cA_6 is inspected for values a_j such that $|a_j| > \frac{3}{2}\sigma_{cA}$. cD_6 is inspected for values d_j such that $|d_j| > \frac{3}{2}\sigma_{cD}$.

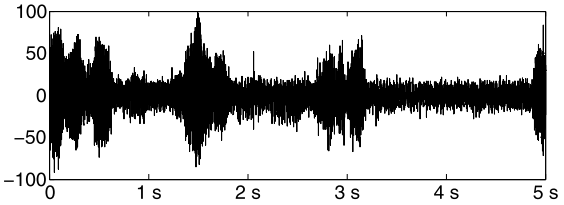

Fig. 19. Raw microelectrode recording.

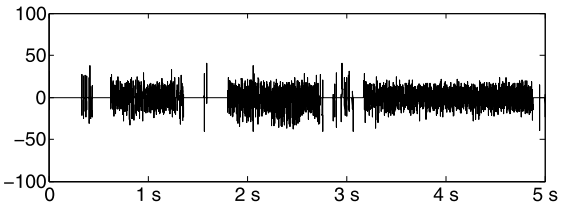

Fig. 20. Microelectrode recording with artifacts removed.

Samples of the original signal that fall in ranges corresponding to found a_j and d_j are set to 0. Later from non zero samples of such modified signal the σ is calculated. Finally, signal is hard thresholded with value 6σ.

2.4.2. Results

Figures 19 and 20 shows results of artifacts removal on 5 s long highly contaminated sample signal. Looking at the raw MER recording it can be perceived that areas contaminated with artifacts have appearance distinctly different from the rest of the signal. Comparing contaminated and filtered signal shows that while artifacts have all been removed, remaining portions of the signal have been left unchanged. Looking at the first second of the recording one may also find that in some cases it is even possible to retain some of the original signal from the contaminated areas. This would have not been possible if only amplitude based filtering methods were applied.

2.5. Analysis of the RMS value

STN is known to produce lots of spikes with high amplitude but also has loud background noise [18] and [19]. It can be expected that signals recorded from it would present elevated Root Mean Square Value. This parameter is, among others, also used for Bayesian calculations in [17]. Assume, that electrode e at depth d recorded n samples $X = x_0, \ldots, x_{n-1}$ and that RMS formula is given by Eq. (13).

$$RMS(e,\ d,\ X) = \sqrt{\frac{\sum_{i=0}^{n-1} x_i^2}{n}} \tag{13}$$

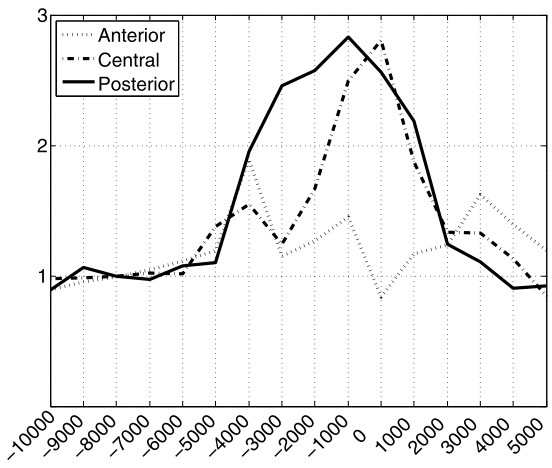

Fig. 21. RMS value chart.

RMS approach is much less computationally demanding than spike detection and can be easier available. It still requires calculation of a sum of squares for all samples from a given recording. Because all samples contribute to the resulting value, this method takes into account both background noise and spikes. If the signal is contaminated by artifacts, the method may produce falsely high RMS values.

2.5.1. Results

Chart with RMS values for the same trial that was used in Fig. 16a is shown on Fig. 21.

Because the method is not spike detection dependant, it should not and is not affected by value jumping that was a clear drawback of the described earlier spike based method. Subsequent RMS values change in a much smoother and less chaotic way. Spike based method (Section 2.3.8) estimated that both $posterior$ and $central$ electrodes might have traversed the STN. RMS based method as shown on Fig. 21 in a clear way assesses that $posterior$ electrode is better than $central$. Both methods show that $anterior$ electrode only briefly enters STN most forward tip at -4000 and then stays outside of it. RMS method defines clear dorsal border of the STN at -4000 with subsequent increase of the RMS up to depth -1000. On greater depths the RMS slowly decreases, placing ventral border around depth of 3000. Such findings and predicted thickness agree with clinical observations found in [1].

2.6. Analysis of the percentile value – PRC

Spikes amplitude is by far greater than the background noise. Because of that one can find an ampli-

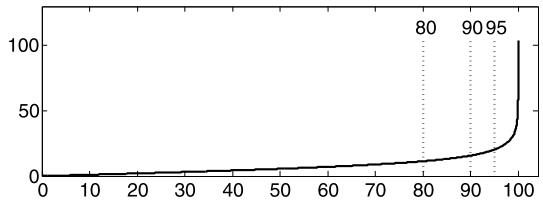

Fig. 22. Amplitude distribution.

tude value below which no spikes are present or above which spike must rise. This feature is commonly used in many neurological appliances, for example the 50th percentile – $median$ of amplitude's module is used for both spike detection and artifact removal process. The approach in which 50th percentile ($median$) of amplitude's module together with other features is used for detecting increased neural activity can be found in [20]. Figure 22 shows amplitude's module distribution for a STN recorded signal. It is obvious that high amplitude ranges that comes from spikes lies after the 95th percentile. Certain percentile value calculated from module of amplitude can thus be used to estimate the amount of background neural activity.

2.6.1. Results

Already the 95th percentile shows background activity and discards almost all samples from the spikes. To be however safely independent from any spike activity, even lower percentile can be used. In this paper the 80th percentile is used.

Figure 23 shows how the value of different percentiles change with subsequent depths. The STN area (roughly spanning from -4000 to $+3000$) characterizes with elevated background activity which is visible as increased percentile value. While lower percentiles (even median) can also be used for such measurement, it must be noted that the lower is the selected percentile, the smaller and less pronounced are the changes in its value between different brain areas.

Having selected 80th percentile as a value that can be used for STN distinguishing an electrode comparison chart can be made. Using the same data set that was used for creation of Fig. 16a and Fig. 21, we obtained following results (Fig. 24).

Obtained results are in full agreement with those given by RMS method. Both methods state that the best electrode is $posterior$ and that STN ranges roughly between -4000 and $+3000$. Decrease of percentile value is somewhat more steep than in the case

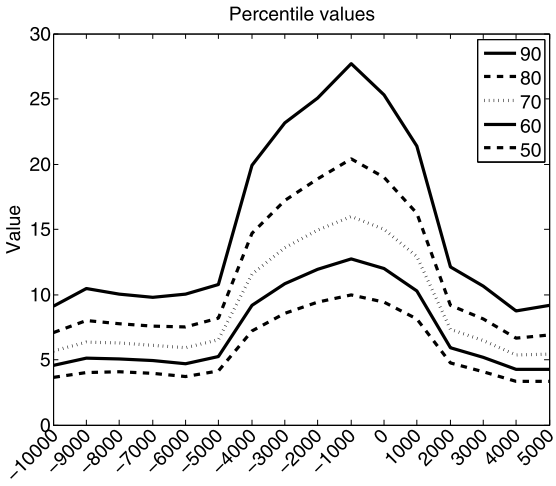

Fig. 23. Percentile value changes.

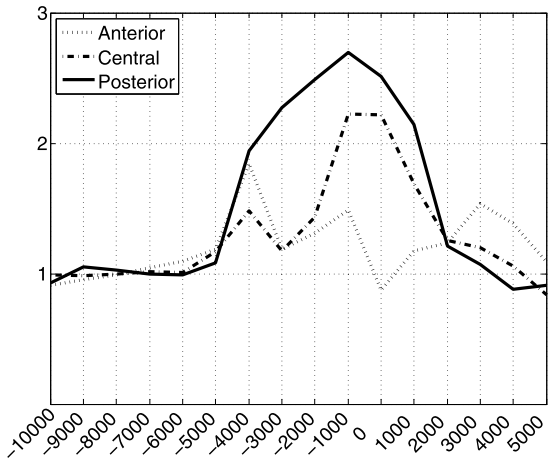

Fig. 24. 80th percentile changes for electrode set.

of RMS, which identifies the ventral border of the STN a bit more clearly.

2.7. DWT based analysis of the LFB power

It has been postulated in [21] and [22] that background neural activity can be divided into two frequency areas. First, an activity in range below 500 Hz is called Low Frequency Background (LFB). Second contains frequencies in range 500 Hz to 3000 Hz and is thus called High Frequency Background (HFB). In mentioned paper authors use properties of HFB to pinpoint STN location. Here, in this section a LFB based method for finding the STN is shown.

As with Quantile based estimator, here too, it is very important to remove as much of the artifacts as pos-

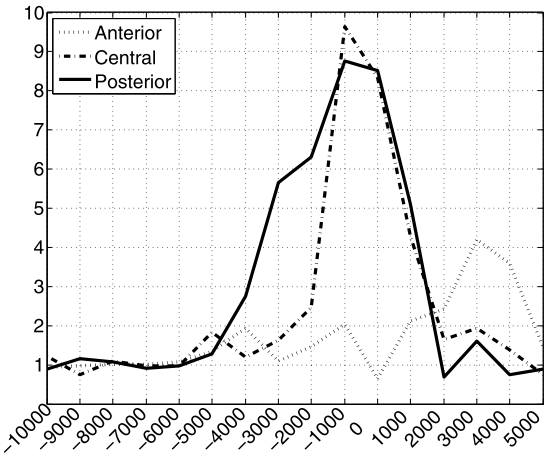

Fig. 25. LFB changes for electrode set.

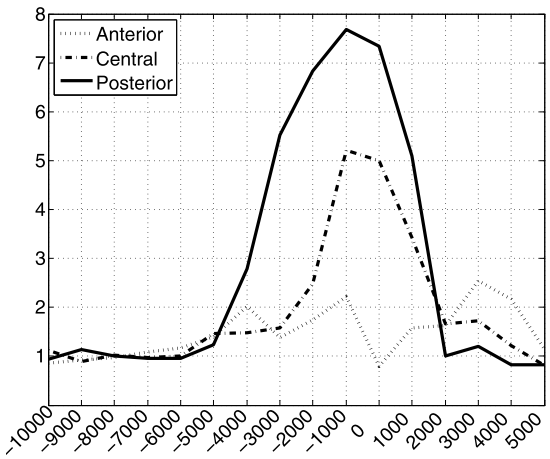

Fig. 26. HFB changes for electrode set.

sible. This is due to the fact that most of the power carried by such artifacts resides in range below 375 Hz that if fully included in the described analysis. Before the transformation can be made, any spikes detected during meta signal construction process are removed from the raw MER recorded signal. Later to ensure removal of even hight distorted spikes, signal is also hard thresholded with value of 80th percentile. After artifacts and spikes have all been removed, similarly as in the case of cited HFB analysis, signal has to be transformed first from time to frequency domain. Here, however instead of FFT the DWT is used. This time DWT is performed fully, i.e. all available forward steps are done. As the result, following list of wavelet coefficient sets is produced: cA_n, cD_n, cA_{n-1}, …, cD_1. Each set of coefficients corresponds to specific frequency range. It is possible to select only those sets for whom their frequency range falls into 0–500 Hz range. Signal's power is subsequently calculated from those sets in a way akin to getting power from FFT results.

2.7.1. Results

One again the LFB power is calculated for the same set of electrodes that were used in previous sections. Results containing LFB power for electrodes and depths are shown on Fig. 25.

Obtained results are in full agreement with those given by RMS and percentile methods. All methods state that best electrode is $posterior$. RMS and percentile based methods estimated STN to be between -4000 and $+3000$. LFB based method further refines this area. STN is to be located between -4000 and $+1000$, this yields thickness of about 5 mm which is in accordance with brain anatomy [2]. What is especially worth mentioning is the visible division of STN into two different parts. Dorsal part spans -4000 to -2000 and has lower power output. Ventral part spans from -1000 to $+1000$ and is definitively more active.

This subdivision of STN and greater activity in the ventral part comes form the fact that STN itself is subdivided into smaller subregions. One of them – ventral part of STN plays crucial role in motor neural circuits and is especially hyperactive in PD patients [1]. Also crossing of LFB amplitudes of $anterior$ and $posterior$ electrode at depth $+2000$ might be due to the border expected here between different brain structures (STN and SNr[5]) [1].

2.8. DWT based analysis of the HFB power

In this section a modified version of the HFB calculation described in [21] and [22] is presented. Difference comes from assumption held also in other sections. MER recorded signals are highly non stationary and so better suited for DWT based filtering. All principles regarding calculation of HFB and LFB are the same, only difference lies in frequency range. For HFB inspected frequency range is between 500 and 3000 Hz.

2.8.1. Results

After calculating HFB for test set of electrodes results shown on Fig. 26 were obtained.

One again, obtained results are in full agreement with those given by RMS, percentile and LFB meth-

[5] SNr – Substantia nigra.

ods. There are two notable differences. Firstly, the $posterior$ electrode is shown as the best one in even more profound way. Secondly, HFB does not show subdivisions of STN nucleus.

3. Evaluation and discussion

3.1. Comparison of methods

Summarizing previous sections, five different methods allowing localization of the STN has been described.

- Meta signal based
  - Does not rely on signal amplitude
  - Not affected by signal artifacts
  - Requires high and low pass filtered signal
  - Relies solely on spike detection and is dependant on electrode being near active cell
  - No discrimination between STN and SNr
- RMS based
  - Not affected by electrode placement
  - Requires high pass filtered signal
  - Strongly affected by signal artifacts
- Percentile based
  - Not affected by electrode placement
  - Requires high pass filtered signal
  - Strongly affected by signal artifacts
  - Good discrimination between STN and SNr
- LFB based
  - Not affected by electrode placement
  - Does not require prior signal filtering
  - Affected by signal artifacts
- HFB based
  - Not affected by electrode placement
  - Does not require prior signal filtering
  - Affected by signal artifacts

Each of the above methods have some advantages and disadvantages.

First of them is not affected by signal artifacts, but on the other hand it is in some way probability based. It cannot also distinguish between STN and SNr (both structures produce high amount of spiking). Because of that it can not be reliably used for classification of single recordings. High coefficient value can be due to electrode being both in STN or SNr. Due to unfavorable electrode placement coefficient value can sometimes be low even for the STN area. It can however be useful when deciding on the electrode level, i.e. whether electrode passed through STN or not. Predictions based on cumulative power have been proven to achieve good results [23].

RMS and Percentile (PRC) based methods can be used for classification of single recordings. Their results can by however completely wrong if signal contains any artifacts. If the artifacts are present during first five recordings, the C_{base} (see Eq. (2)) can be set so high that the actual STN location would not be detected at all.

LFB and HFB based methods both rely on frequency analysis. They do not require prior filtering. In fact no prior filtering should take place. In some recording systems the frequencies below 500 Hz are automatically removed. When such recording is analyzed, the LFB method is of course unusable.

3.2. Recording clustering

Using the RMS, PRC, LFB and HFB methods, each recording d made by some electrode at given depth has the set of coefficients described by Eq. (14)

$$C = \left\{c_{RMS}(d), c_{PRC}(d), c_{LFB}(d), c_{HFB}(d)\right\} \quad (14)$$

Having this coefficients, an attempt to obtain meaningful clustering of the recording has been done. Clusterings, as described in [24] reflects the natural grouping of the objects and are frequently applied in biology and medicine. Assumption was, that recordings can be divided into three clusters containing respectively:

α – recordings made outside the STN
β – recordings made in areas near the STN
γ – recordings made inside the STN

Clustering has been done using hierarchical cluster tree with Euclidian distance and minimum variance algorithm. As input to the clustering procedure all possible 2, 3 and 4 – element subsets of C has been tried. This produced $\binom{4}{2} + \binom{4}{3} + \binom{4}{4} = 11$ clusterings.

Table 1 shows for each chosen subset the percentage distribution of recordings. Calculated Spearman rank value for the Cophenetic correlation coefficient is also included. Regardless of the coefficients subset taken for clustering, the Spearman rank is greater than 0.86 and in most cases it is above 0.9. This ensures that pro-

Table 1
Clustering summary

Input coefficients	Cluster α size	Cluster β size	Cluster γ size	Spearman rank
RMS, PRC	72.95 %	17.71 %	9.33 %	0.862
RMS, LFB	72.85 %	21.74 %	5.42 %	0.905
RMS, HFB	74.19 %	17.04 %	8.77 %	0.926
PRC, LFB	85.67 %	8.60 %	5.73 %	0.907
PRC, HFB	65.74 %	22.55 %	11.71 %	0.907
LFB, HFB	85.00 %	12.75 %	2.25 %	0.910
PRC, LFB, HFB	82.08 %	12.19 %	5.73 %	0.907
RMS, LFB, HFB	71.59 %	18.17 %	10.25 %	0.911
RMS, PRC, HFB	73.72 %	23.80 %	2.47 %	0.877
RMS, PRC, LFB	85.31 %	9.08 %	5.61 %	0.906
RMS, PRC, LFB, HFB	75.78 %	18.93 %	5.30 %	0.885

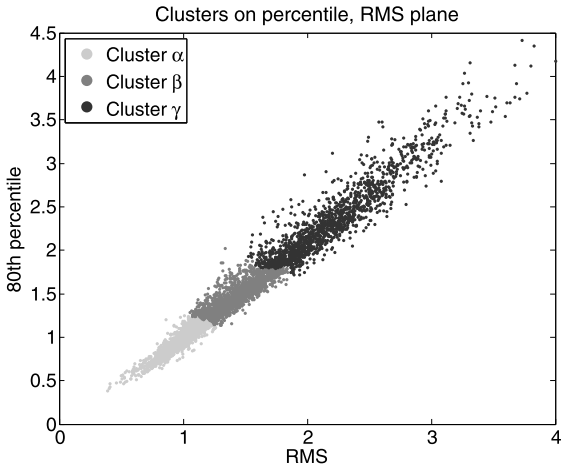

Fig. 27. Clustering with RMS and PRC shown of RMS, PRC plane.

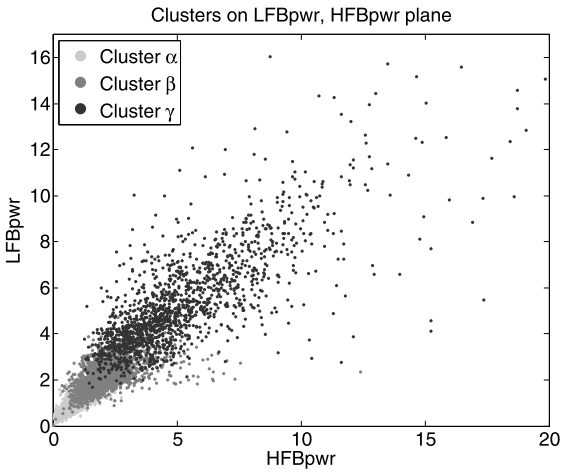

Fig. 28. Clustering with RMS and PRC shown of LFB, HFB plane.

duced clustering was of good quality. Cluster size also seem to be stable. Having $\mu_\alpha = 76.8$, $\mu_\beta = 15.6$ and $\mu_\gamma = 6.6$ and $\sigma_\alpha = 6.3$, $\sigma_\beta = 5$ and $\sigma_\gamma = 2.9$ one can observe that for B and C clusters over 80 % of observation fall within $(\mu - \sigma,\ \mu + \sigma)$ range.

3.2.1. Cluster cross comparison

On the following pictures some of the more interesting clustering results are shown. Especially interesting are the results obtained when clustering was made using one subset of coefficients and clustering results are also shown using another subset.

Figure 27 shows results of the clustering done using only coefficients c_{RMS} and c_{PRC}. One can clearly observe that data set has been divided into three sections.

Cluster α – very dense and numerous, containing recordings assumed to be made outside of the STN (around 7000 of recordings).

Cluster β – much less dense, containing recordings assumed to be made near the STN (while having area similar to cluster A, it contains only around 1700 recordings).

Cluster γ – sparse, containing recordings that are assumed to be coming from the STN (contains only about 900 recordings).

Figure 28 shows results of the same clustering that is shown on Fig. 27. It shows however a recording seen from the point of view of other two coefficients (c_{LFB} and c_{HFB}). One can plainly see the cluster α that contains recordings made outside STN. As expected, the recording from that cluster have also small c_{LFB} and c_{HFB} values. Also, as expected, recordings from cluster γ are characterized by largest in population values of c_{LFB} and c_{HFB}. This is a clear evidence that obtained results are stable and regardless of chosen coefficient subset recordings are divided in a similar way.

Table 2
μ fraction of common elements between clusters

	α	β	γ
α	0.959	0.041	<0.0003
β	0.181	0.709	0.110
γ	0.003	0.211	0.785

Table 3
σ fraction of common elements between clusters

	α	β	γ
α	0.053	0.053	0.001
β	0.233	0.228	0.150
γ	0.011	0.239	0.242

Taking $C_1 \subseteq C$ and $C_2 \subseteq C$ (see Eq. (14)) the resulting α_1 and α_2 clusters in worst case scenario have over 77 % common elements. As it can be seen in Table 1, results produced by clustering on PRC and HFB differ considerably from other results. Removing from consideration these clusterings raised fraction of intersection to 84 %. Now fraction of elements common in α clusters has mean $\mu = 0.959$ with $\sigma = 0.053$. Fraction of elements common in β clusters has mean $\mu = 0.709$ with $\sigma = 0.228$. Fraction of elements common in γ clusters has mean $\mu = 0.785$ with $\sigma = 0.242$.

Results in Tables 2 and 3 show good clustering stability. On average only 4.1 % of recordings classified by one clustering to cluster α could be placed by another clustering into β. Even less of them, around 0.03 % can fall info γ cluster. Also the other way round, only around 1.1 % of recordings classified by one clustering to cluster γ could be placed by another clustering into α. This allows one to say with good certainty that obtained results are comparable between clusterings. Recording that has been assigned with cluster label α is much, much less likely to come from the STN than another one with cluster label β – even if labels come from different clusterings.

3.3. Review of clustering results

Let us introduce ranking between clusters. As our goal is to find the STN, the most natural order is that γ is favorable to β which is also favorable to α. Having done that, assume that for given recording, best cluster is the most favorable cluster among all assignments made by different clusterings.

Table 4
Cluster assignments for $Anterior$ electrode

depth	-10	-9	-8	-7	-6	-5	-4	-3
best cluster	α	α	α	α	α	α	β	α
depth	-2	-1	0	$+1$	$+2$	$+3$	$+4$	$+5$
best cluster	β	β	α	2	β	β	β	α

Table 5
Cluster assignments for $Central$ electrode

depth	-10	-9	-8	-7	-6	-5	-4	-3
best cluster	α	α	α	α	α	α	β	β
depth	-2	-1	0	$+1$	$+2$	$+3$	$+4$	$+5$
best best cluster	β	γ	γ	β	β	β	α	α

Table 6
Cluster assignments for $Posterior$ electrode

depth	-10	-9	-8	-7	-6	-5	-4	-3
best cluster	α	α	α	α	α	α	β	γ
depth	-2	-1	0	$+1$	$+2$	$+3$	$+4$	$+5$
best cluster	γ	γ	γ	γ	α	α	α	α

3.3.1. Case one

Let us take the example pass of electrodes that was shown in Sections 2.5, 2.6, 2.7 and 2.8. Figures 29a, 29b, 29c and 29d are scaled down versions taken from above sections and are placed here for easier comparison with clustering results. Each electrode produced 16 recordings (from depths ranging $-10000\,\mu$m to $5000\,\mu$m).

For compactness, depths in Tables 4, 5 and 6 are shown in mm not in μm. Table 4 shows how recordings made by $Anterior$ electrode were classified. Table 5 show how recordings made by $Central$ electrode were classified. Table 6 show how recordings made by $Posterior$ electrode were classified.

$Anterior$ electrode has no recordings labeled as γ and largest continuous β sequence contains three depths.

$Central$ electrode has two subsequent depth labeled as γ, they together with adjacent β recordings form 8 element sequence.

$Posterior$ electrode has five subsequent depth labeled as γ, they together with adjacent β recordings form 6 element sequence.

Basing on obtained results, as the best electrode we select the $Posterior$ one – it contains largest sequence of γ labeled recordings. As $Anterior$ electrodes pro-

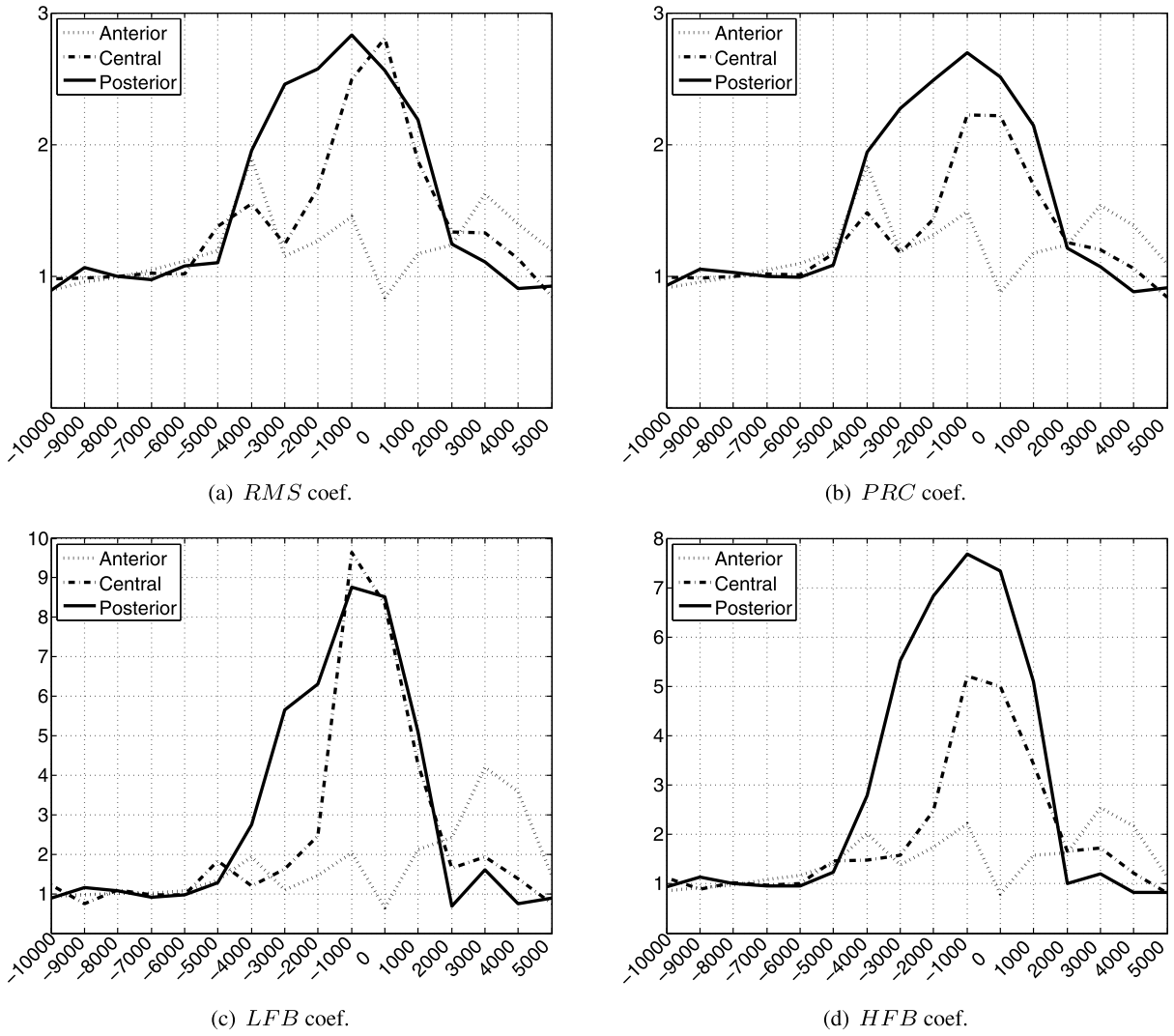

(a) RMS coef. (b) PRC coef.

(c) LFB coef. (d) HFB coef.

Fig. 29. Coefficients for selected pass of electrodes.

duced no recordings labeled as γ, the 2nd best would be of course the $Central$ electrode.

3.3.2. Case two

The following example has been specially chosen to show situation when STN is visible on calculated results, but relative coefficients values are not so high.

Looking at Fig. 30 there are certain similarities to Fig. 29a, there is however a significant difference. RMS amplitude in this case fits for all electrodes beneath value 1.8 while in previous one for some electrodes it was around 2.75. Of course amplitudes in both cases (see Section 2.2) are normalized according to average from first five depths. Reason for such a big – around 50 % – difference in RMS value can be various. It can be both electronically and physiologically based. It is for example possible, that in a subject case the STN nucleus was simply less active then in the first patient.

On Fig. 31 too, similar as with RMS values, differences can be observed. Normalized amplitude of PRC coefficient in the first case was around 2.75 while for second patient it reached only to around 1.7.

In the case of LFB differences are even more profound, normalized LFB values for 1st patient reached value of 10. For 2nd case LFB amplitude is at all depths below value of 3. Comparing the larger version of Fig. 29c (Fig. 25) with Fig. 32 it becomes obvious that even the worst electrode from the first patient has LFB at some depth values larger than 3. This poses

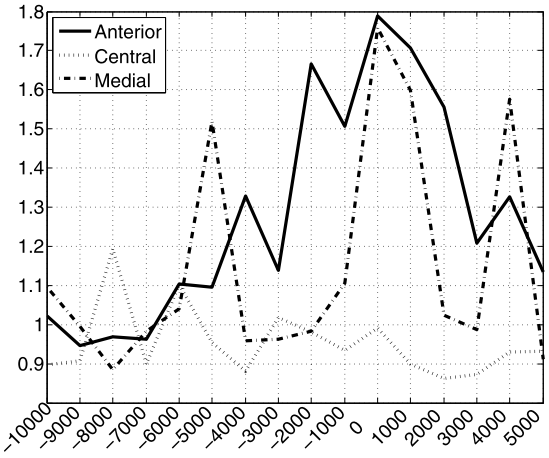

Fig. 30. RMS coefficient.

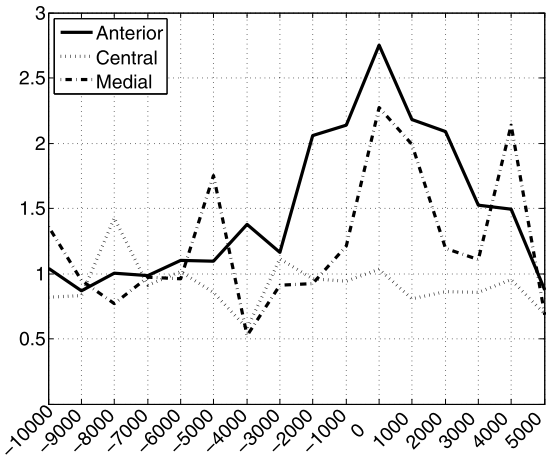

Fig. 32. LFB coefficient.

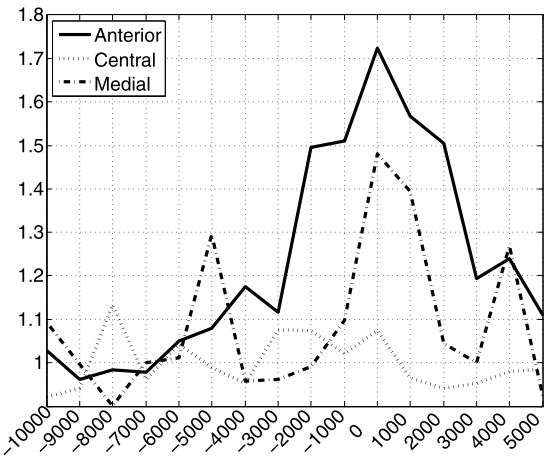

Fig. 31. PRC coefficient.

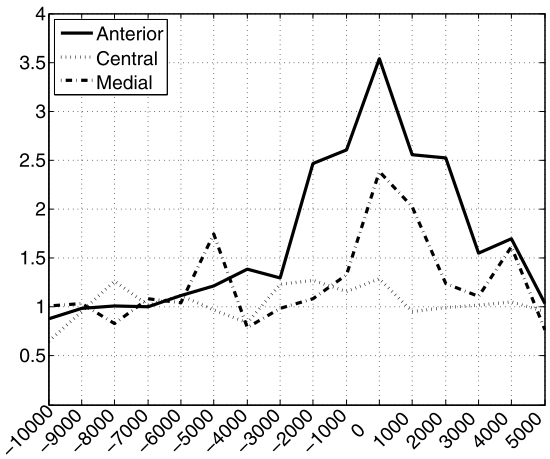

Fig. 33. HFB coefficient.

an issue that has to be addressed. The same value of a given coefficient in the first patient was clearly too low to indicate STN while being large enough in the second.

HFB values also exhibit the same issue. Normalized HFB values for the first patient reached almost the value of 8 while in the second patient they are all contained below value of 4.

Such big differences must have some implications in clustering results. And, yes, indeed it has. As seen in Tables 7, 8 and 9, none of the recordings has been assigned the γ label. Such situation is not a frequent one. In reviewed 163 trials (each trial represents a single pass of electrode array through a brain hemisphere), only in 24 (14.7 %) of them there were no electrodes that produced at least one recording labeled as γ. In absence of γ recordings, ones labeled as β must be used. Table 7 shows how recordings made by $Anterior$ electrode were classified. Table 8 shows how recordings made by $Central$ electrode were classified. Table 9 show how recordings made by $Posterior$ electrode were classified.

$Anterior$ electrode contains 5 elements long sequence of recordings labeled as β.

Table 7
Cluster assignments for $Anterior$ electrode

depth	-10	-9	-8	-7	-6	-5	-4	-3
best cluster	α	α	α	α	α	α	α	α
depth	-2	-1	0	$+1$	$+2$	$+3$	$+4$	$+5$
best cluster	β	β	β	β	β	α	β	1

Table 8
Cluster assignments for $Central$ electrode

depth	-10	-9	-8	-7	-6	-5	-4	-3
best cluster	α	α	α	α	α	α	α	α
depth	-2	-1	0	$+1$	$+2$	$+3$	$+4$	$+5$
best cluster	α	α	α	α	α	α	α	α

Table 9
Cluster assignments for $Medial$ electrode

depth	-10	-9	-8	-7	-6	-5	-4	-3
best cluster	α	α	α	α	α	β	α	α
depth	-2	-1	0	$+1$	$+2$	$+3$	$+4$	$+5$
best cluster	α	α	β	β	α	α	β	α

$Central$ electrode produced no recordings labeled as β.

$Medial$ electrode has only 2 element long sequence of recordings labeled as β.

Basing on obtained results, as the best electrode selected was the $Anterior$ one – it contains largest sequence of β labeled recordings. As $Central$ electrodes produced no recordings labeled as γ, the 2nd best would be the $Medial$ electrode.

3.4. Electrode ordering

Having labeled the recordings, we can now offer a way to rank them as to how good did they reached/passed through the STN. For this, we define three measures defined for an electrode:

- $M_\gamma 1$ – count of recordings labeled as γ.
- $M_\gamma 2$ – length of the longest sequence of recordings labeled as γ.
- $M_{\gamma\beta}$ – length of the longest sequence of recordings labeled as γ or β.

Electrodes are then ordered as follows: firstly in descending order according to M_γ value, on the second level descending according to $M_{\gamma\beta}$ value and finally, descending according to M_β.

Table 10 contains example of such ranking using defined measures.

Rank finds its confirmation also in coefficients values. Figure 34 shows value of LFB for electrodes described in Table 10.

3.4.1. Cluster based vs meta power ordering

Comparing electrode rankings produced by analysis of meta power and by coefficient clustering shows

Table 10
Electrode rank example

Electrode	Recording clusters	$M_{\gamma 1}$	$M_{\gamma 2}$	$M_{\gamma\beta}$
Anterior	$\alpha\alpha\alpha\alpha\alpha\alpha\alpha\alpha\beta\gamma\beta\gamma\beta\beta\beta\beta$	2	1	8
Posterior	$\alpha\alpha\alpha\alpha\alpha\alpha\beta\beta\beta\beta\beta\gamma\beta\beta\alpha\beta$	1	1	8
Medial	$\alpha\alpha\alpha\alpha\alpha\alpha\alpha\beta\beta\gamma\beta\beta\alpha\beta\alpha\alpha$	1	1	5
Central	$\alpha\alpha\alpha\alpha\alpha\alpha\alpha\beta\beta\beta\beta\beta\beta\beta\beta\beta$	0	0	9

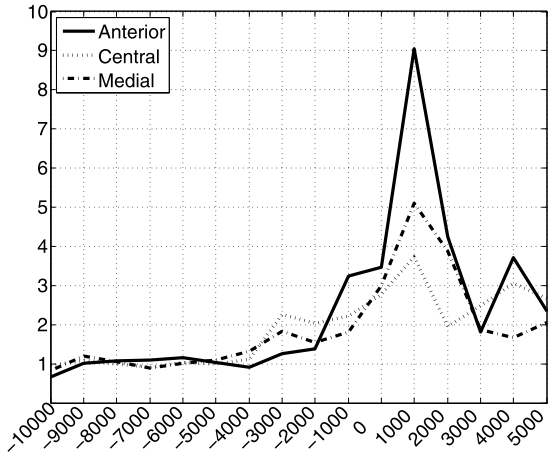

Fig. 34. LFB coefficient.

that although results are in some way similar there are also notable differences. When comparing ranks of 550 electrodes, it emerged that in 415 (75.45 %) cases rank has not changed or changed by one position.

There were 326 electrodes with 1st or 2nd rank assigned by meta power method. 338 electrodes have 1st or 2nd rank assigned by cluster based method. Intersection of both sets give electrodes that have been selected as best or 2nd best by each approach. This resulting set contains 217 electrodes, it is 66 % when comparing to meta power results and 64 % when comparing to cluster method results. Differences in both sets come from issue explained in Section 2.3.8. Figure 16a shows summary meta power for certain trial of electrodes. It is evident that two electrodes $Posterior$ and $Central$ have elevated summary power at depths around -2000. Third electrode – $Anterior$ – however has medium power throughout almost all of passage and as the result its cumulative power is the greatest one. So, the ordering of electrodes produced by meta power is $Anterior$, $Posterior$, $Central$. Order produced by clustering is free from that influence and is $Posterior$, $Central$, $Anterior$ which is of course more true.

4. Conclusion

There are several ways in which given recordings can be classified as coming from STN or not. They all have their advantages and disadvantages. Spike based methods like meta power, intra spike histogram[1] or simple spike count must rely on spike detection. This can be difficult due to the nature of MER recorded signal. Low frequency components or artifacts can lead to incomplete detection of spikes. On another hand – as shown in Section 2.3.8 – STN is not the only area characterized by high spiking activity. This could led to both false negative and false positive detections of the STN.

Other classes of methods, especially RMS, PRC, LFB and HFB described in this paper do not directly rely on spike detection. They of course require some signal preprocessing. Especially essential is artifact removal. Each of them helps to find the STN location using different approach, still, as pointed out in Section 3.2.1 they greatly agree in their assessments. Hierarchical clusterings that base on the described methods proved to be an effective method for STN discrimination. Obtained results are more stable, accurate and less probability dependant then those basing on spikes. This all, proves that it is possible to construct autonomic and automatic decisive support system for STN detection. It's because low specificity might lead to false-positive result. It might identify a wrong area of a brain as a good for electrode implantation. Such erroneous placement of electrode might lead to tragic disturbance of patient's emotions [1].

Acknowledgements

Authors would like to thank the reviewers for their suggestions.

References

[1] Z. Israel and K.J. Burchiel, *Microelectrode Recording in Movement Disorder Surgery*, Thieme Medical Publishers, 2004.

[2] J. Nolte, *The Human Brain, An Introduction to Its Functional Anatomy*, Elsevier, 2009.

[3] I.M. Khademul, I. Rabiul, T. Toshihisa, and T.M. Rutkowski, Artifact suppression from EEG signals using data adaptive time domain filtering.

[4] O. Bertrand, J. Bohorquez, and J. Pernier, Time-frequency digital filtering based on an invertible wavelet transform: An application to evoked potentials, *IEEE Transactions on Biomedical Engineering* **41**(1) (1994), 77–88.

[5] F.E. Turkheimer, J.A. Aston, R.B. Banati, C. Riddell, and V.J. Cunningham, A linear wavelet filter for parametric imaging with dynamic PET, *IEEE Transactions on Medical Imaging* **22**(3) (2003), 289–301.

[6] A. Pižurica, A.M. Wink, E. Vansteenkiste, W. Philips, and J.B.T.M. Roerdink, A review of wavelet denoising in MRI and ultrasound brain imaging, *Currrnt Medical Imaging Reviews* **2**(2) (2006), 247–260.

[7] A. Jensen and A. Cour-Harbo, *Ripples in Mathematics*, Springer-Verlag, 2010.

[8] A.B. Wiltschko, G.J. Gage, and J.D. Berke, Wavelet filtering before spike detection preserves waveform shape and enhances single-unit discrimination, *Journal of Neuroscience Methods* **173**(1) (2008), 34–40.

[9] S.W. Smith, *Digital Signal Processing*, Elsevier, 2003.

[10] K.H. Pettersen and G.T. Einevoll, Amplitude variability and extracellular low-pass filtering of neuronal spikes, *Biophysical Journal* **94**(3) (2008), 784–802.

[11] D.L. Donoho, De-noising by soft-thresholding, *IEEE Transactions on Information Theory* **41**(3) (1995), 613–627.

[12] C. Archer, M.E. Hochstenbach, C. Hoede, G. Meinsma, H.G.E. Meijer, A. Ali Salah, C.C. Stolk, T. Swist, and J. Zyprych, Neural spike sorting with spatio-temporal features, in: *Proc. of the 63 European Study Group Mathematics with Industry*, 28 Jan–1 Feb 2008.

[13] S.B. Wilson and R. Emerson, Spike detection: A review and comparison of algorithms, *Clinical Neurophysiology* **113**(12) (2002), 1873–1881.

[14] C. Koch, *Biophysics of Computation: Information Processing in Single Neurons*, Oxford University Press, New York, 1999.

[15] R.S. Stanković and B.J. Falkowskib, The Haar wavelet transform: Its status and achievements, *Computers & Electrical Engineering* **29**(1) (2003), 25–44.

[16] R.Q. Quiroga, Z. Nadasdy, and Y. Ben-Shaul, *Unsupervised Spike Detection and Sorting with Wavelets and Superparamagnetic Clustering*, MIT Press, 2004.

[17] A. Moran, I. Bar-Gad, H. Bergman, and Z. Israel, Real-time refinement of subthalamic nucleus targeting using bayesian decision-making on the root mean square measure, *Movement Disorders* **21**(9) (2006), 1425–1431.

[18] G. Pizzolato and T. Mandat, Deep brain stimulation for movement disorders, *Frontiers in Integrative Neuroscience* **6**(2) (2012).

[19] S. Hemm and K. Wøardell, Stereotactic implantation of deep brain stimulation electrodes: A review of technical systems, methods and emerging tools, *Medical & Biological Engineering & Computing* **48**(7) (2010), 611–624.

[20] P. Gemmar, O. Gronz, T. Henrichs, F. Hertel, and C. Decker, MER classification for deep brain stimulation, in: *Proc. of the Sixth Heidelberg Innovation Forum*, Apr 2008.

[21] P. Novak, S. Daniluk, S.A. Ellias, and J.M. Nazzaro, Detection of the subthalamic nucleus in microelectrographic recordings in Parkinson disease using the high-frequency (>500 Hz) neuronal background, *Journal of Neurosurgery* **10**6(1) (2007), 175–179.

[22] P. Novak, A.W. Przybyszewski, A. Barborica, P. Ravin, L. Margolin, and J.G. Pilitsis, Localization of the subthalamic nucleus in Parkinson disease using multiunit activity, *Journal of the Neurological Sciences* **310**(1–2) (2011), 44–49.

[23] K. Ciecierski, Z.W. Raś, and A.W. Przybyszewski, Selection of the optimal microelectrode during DBS surgery in Parkinson's patients, in: *Foundations of Intelligent Systems*, Lecture Notes in Computer Science, Vol. 6804, 2011, pp. 554–564.

[24] X. Xu, L. Chen, and P. He, A novel ant clustering algorithm based on cellular automata, in: *Proc. of the IEEE/WIC/ACM International Conference on Intelligent Agent Technology, (IAT 2004)*, 2004.